Journal of Engineering and Technology for Industrial Applications

ITEGAM-JETIA

Manaus, v.8 n.34, p. 20-28. Mar/Apr, 2022

DOI: https://doi.org/10.5935/jetia.v8i34.805

ISSN ONLINE: 2447-0228

RESEARCH ARTICLE OPEN ACCESS

MULTIOBJECTIVE OPTIMIZATION OF CUTTING PARAMETERS FOR FINISHING END MILLING HARDOX® 450

Émerson S. Passari[1], Heraldo J. Amorim[2] and André J. Souza*[3]

[1, 2, 3] Department of Mechanical Engineering (DEMEC), Federal University of Rio Grande do Sul (UFRGS), Porto Alegre, RS, Brazil.

[1] http://orcid.org/0000-0002-8349-1348, [2] http://orcid.org/0000-0002-0498-6378, [3] http://orcid.org/0000-0001-5649-7333

Email: emerson.passari@gmail.com, amorim@mecanica.ufrgs.br, *ajsouza@ufrgs.br

ARTICLE INFO

Article History
Received: April 13th, 2022
Accepted: April 24th, 2022
Published: April 30th, 2022

Keywords:
Hardox® 450,
End milling,
Machining force,
Surface roughness,
Box-Behnken design.

ABSTRACT

Hardox® 450 is pre-hardened structural steel with high hardness and mechanical strength, designed to resist under abrasion wear, cracks, and breakages. This material provides a longer service life for crushers, buckets, and gears due to its excellent mechanical properties, which result in low machinability. Moreover, the knowledge about machining this material is limited, justifying further investigation. Thus, this study aims to evaluate the influence of cutting speed (v_c), axial depth of cut (a_p), and feed per tooth (f_z) on the machining forces and surface finish during the finishing end milling of Hardox® 450 with a CVD-coated carbide tool. The experiment was planned and analyzed through a 3-factor, 3-level Box-Behnken Design. The analysis of variance showed that a_p was the most significant parameter for all response variables considered in this study. A multiobjective optimization was carried out to determine the ideal levels of cutting parameters, considering the lowest values of static and dynamic machining forces and average and total surface roughnesses. The model suggests that the best results are achieved with v_c = 89 m/min, f_z = 0.1 mm/tooth, and a_p = 0.212 mm. Even with efficient results, the predicted and measured response variables differed slightly (mainly due to tool wear).

I. INTRODUCTION

Hardox® 450 is pre-hardened wear-resistant steel manufactured by Oxellösund SSAB (Sweden), with a 45 HRC nominal hardness, 1250 MPa specific yield strength, and 1400 MPa tensile strength. It is known for its high abrasion resistance and good structural properties [1]. Furthermore, this material has a tempered martensite microstructure due to the combination of carbon and alloy elements (Mn, Cr, Ni, Mo, B) [2]. Due to high wear resistance, ductility, and toughness, Hardox® is commonly used to increase the work-life of crushers, buckets, screens, feeders, and gears [3]. However, its high wear resistance implies low machinability, causing a high flank wear rate and, consequently, a short tool life [3, 4].

Since they are considered difficult-to-cut materials, Hardox® steels are usually processed through unconventional machining processes such as abrasive water jet (AWJ), laser, and plasma [5]. Nonetheless, this family of materials is prone to suffer microstructural changes when exposed to temperatures above 250 °C, potentially leading to the degradation of the mechanical properties, especially hardness [6]. Thus, it is recommended to use cold cutting methods such as AWJ, submerged cutting, or direct a cooling fluid spray into the cutting zone when conventional machining processes are used [5, 7]. Since milling is more broadly used and economical than most unconventional machining processes and rarely generates a heat-affected zone in the workpiece [8], some researchers decided to explore the feasibility of using this machining process in the manufacturing of Hardox® steels, some even considering the optimization of the cutting parameters. This approach is widely used to reduce cutting forces and ensure better surface finishing in machining processes.

Krolczyk et al. [9] analyzed the surface topography generated by the processing of Hardox® 400 through different machining processes. The end milling tests were performed with a 4-teeth carbide end mill cutter considering two cutting conditions:

(1) v_{f1} = 80 mm/min and n_1 = 400 rpm, (2) v_{f2} = 160 mm/min and n_2 = 250 rpm. According to the authors, the values of skewness S_{sk} of the samples indicated that the majority of the material is localized in nearby valleys, while the values of kurtosis S_{ku} specified the presence of inordinately high peaks and deep valleys in the surface texture for the sample (1) (S_{ku} > 3). Moreover, the polar graph indicated that the milled surface has an anisotropic periodical structure.

Among the statistical optimization techniques covered, the Taguchi method is one of the most frequently used in milling processes [10] as it allows the study of parameters with only a small number of experiments [11]. Kara [12] studied the cutting parameters through the Taguchi method for the finish end-milling of Hardox® 400 with PVD-coated carbide tools considering two different cutting speeds (60 and 120 m/min) and lubricooling conditions (dry and wet). According to ANOVA, cutting speed is the most significant factor in the roughness values (64.6%) for this study, followed by the lubricooling condition (13.3%). After validation experiments, the optimum R_a value (0.33 µm) was obtained with wet milling and v_c = 120 m/min. It is noteworthy that the DOE applied was equivalent to a 2^2 factorial DOE, which is highly efficient to find the significant influences but neglects any higher-order influence, assuming that all relationships are linear. Since the behaviors between the tested levels are linear, the results provided for experiments that use two levels always point to one of the tested conditions. Moayyedian et al. [13] used the Taguchi method to evaluate the influence of cutting parameters (feed rate v_f, spindle speed n, axial depth of cut a_p, and radial immersion of the tool a_e/d) on the surface roughness after milling Hardox® 600. The results showed that a_e/d presented the most significant influence over the surface roughness, with a contribution of 45.3%. This parameter was followed by n (21.1%), a_p (20.0%), and v_f (13.6%). After optimization, the authors performed a validation test for the optimal condition, whose surface roughness presented a 5.5% error from the result predicted by the model. They mentioned the number of selected parameters for evaluating the surface roughness as the main limitation of this study. However, the DOE used consisted of only nine runs, with confounded iterations and no replication.

Despite the excellent results of the industrial application of the Taguchi method, the information provided by this technique is frequently oriented to results. According to Nekere and Singh [14], the desired requirements are obtained by selecting the best conditions which produce a consistent performance, thus providing a systematic, simple, and efficient methodology for optimizing near optimum design parameters. However, intending to reduce the number of runs, this method often considers the influence of the control variables to be linear due to selecting two levels.

Response surface methodology (RSM) is a group of techniques for analyzing experimental data, and it is frequently used to investigate milling processes [8, 10]. This method involves modeling the response of a system through an n-dimensional surface, whose function, usually a low-order polynomial, can be used to optimize the studied process. RSM is generally used with a suitable design of experiments: CCD (Central Composite Design) and BBD (Box-Behnken Design) are the more usual DOEs. CCD involves the factorial and fractional design, obtaining a complete adjustment of the quadratic model. Although not including such effects, BBD presents the combination of factors in three levels through a reduced number of combinations [15]. BBD allows both statistical optimization and the analysis of the effect of each independent variable (factor) and their combinations on the response variable. The method is based on a combination of factors in three levels: low (-1), medium (0), and high (+1), and provides efficient estimates for first and second-order coefficients, with the advantage of being performed efficiently with fewer samples when compared with full factorial DOEs. For example, for an experiment with three input factors, the number of runs is reduced from 27 (full factorial) to 15 [16].

One of the results of RSM is the generation of regression models for the response variables as a function of the process parameters, a vital part of the optimization process. When predicting the parameters' optimization, the significance analysis of each input factor and its combinations results in ideal process parameters for the required response variable. Therefore, BBD uses the regression coefficients and the probability of significance (p-value ≤ α) to define a variance analysis (ANOVA) considering a confidence interval of 1 – α. In the ANOVA, uncertainties are associated with random and statistical errors in the process and the variables that showed p-value > α (low significance). Thus, as the analysis is debugged, these factors become part of the range of errors, allowing only significant values to be presented. This approach uses a reduced ANOVA that explains only the variables that have significance for the model [17]. In the case of multiobjective optimization, it is possible to contemplate the behavior and influence of all variables present in the study and determine the combination of parameters that meets the criteria expected on the machined surface [3, 16].

Due to the lack of research regarding the milling of Hardox® steels, this work presents a multiobjective optimization of the cutting parameters (v_c, f_z, a_p) in the end milling of Hardox® 450 aiming to minimize the response variables (static and dynamic forces, and surface roughness parameters) simultaneously.

II. MATERIALS AND METHODS

Table 1 presents the chemical composition of the Hardox® 450 samples according to the Manufacturer's Inspection Certificate nº EN 10 204 – 3.1 and the maximum values allowed according to SSAB [1]. Figure 1 presents the micrography of Hardox® 450 steel. Its martensitic microstructure allied with the high manganese content, which induces the work hardening, guarantees Hardox® 450 high hardness, toughness, abrasion resistance, and good weldability due to the low percentage of carbon equivalent [12].

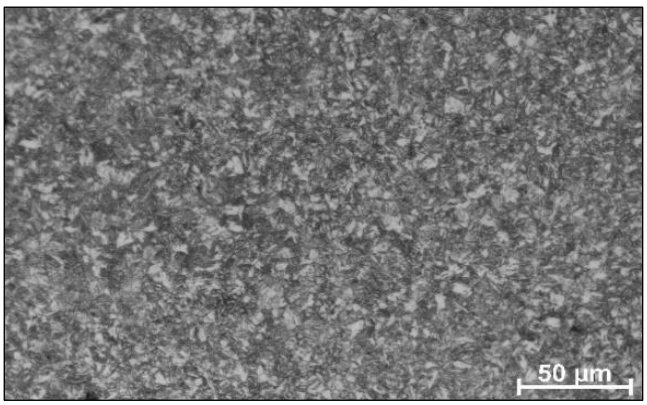

Figure 1: Micrography of Hardox 450 obtained through optical microscopy.
Source: (Courtesy of Welding and Related Techniques Laboratory, UFRGS, Brazil, 2021).

The experiments were executed on three rectangular samples with 100 x 90 x 3.5 mm, extracted from the same sheet, with holes for fixturing on the dynamometer. Six 34 mm runs (samples) were machined in each specimen. Due to the thickness of the samples, only one face was machined.

Table 1: Chemical Composition of the Workpiece (% mass).

	C	Si	Mn	P	S	Cr	Ni	Mo	B	Others
Certificated	0.177	0.170	1.29	0.011	0.001	0.25	0.05	0.02	0.0015	0.073
Normalized	0.260	0.700	1.60	0.025	0.010	1.40	1.50	0.60	0.0050	–

Source: Authors, (2022).

End-milling tests were performed in a ROMI Discovery 308 machining center using Walter Tools WKP35S CVD-TiCN/Al_2O_3 coated carbide inserts with r_ε = 0.4 mm fixed on a 2-insert Walter Tools Xtra-tec tool holder with a length of 35 mm and diameter of 20 mm. Bondmann BD-Fluid B90 oil-free bio-lubricant (1:20 dilution) was applied in abundance throughout the experiments.

The orthogonal components of the machining force (F_x, F_y, F_z) were measured with a Kistler 9129A piezoelectric dynamometer and conditioned with a Kistler 5070A charge amplifier. The force signals were acquired through a Measurement Computing PCIM-DAS 1602/16 DAQ at a 5 kS/s rate and processed digitally by the LabVIEW®9.0 software on a dedicated computer. MS Excel was used for the analysis and postprocessing of the force signals. Figure 2 illustrates the experimental setup.

For the processing data of the machining force, the tool input and tool output were neglected due to the unstable cut in this region. The resulting force (F_R) was calculated by equation 1, while the active (F_a) and passive (F_p) forces by equation 2. The data were processed to obtain the static and dynamic machining forces [18]. The static force (F_U) denotes the root mean square (RMS) value of F_R for the steady sampling interval (S = 2000) is given by equation 3, while the dynamic force (dF_U), which represents the fluctuation of the force around the static force (considering the Normal distribution with 95% confidence interval), is given by equation 4.

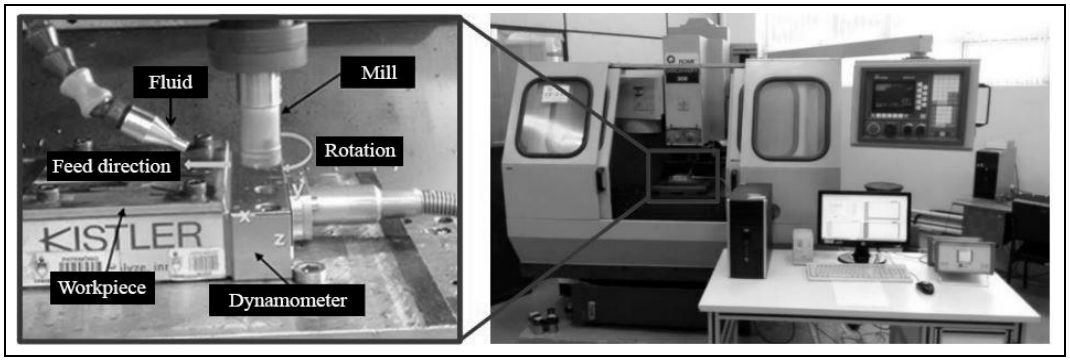

Figure 2: Experimental setup.
Source: Authors, (2022).

$$F_R = \sqrt{F_x^2 + F_y^2 + F_z^2} \quad \text{and} \quad F_R = F_U \pm dF_U \tag{1}$$

$$F_a = \sqrt{F_x^2 + F_y^2} \quad \text{and} \quad F_p = F_z \tag{2}$$

$$F_U = \sqrt{\frac{\sum_{i=1}^{S} F_{Ri}^2}{S}} \tag{3}$$

$$dF_U = 1.96\sqrt{\frac{\sum_{i=1}^{S}\left(F_{Ri} - \bar{F}_R\right)^2}{S}} \quad \text{where} \quad \bar{F}_R = \frac{\sum_{i=1}^{S} F_{Ri}}{S} \tag{4}$$

The machined surface texture (roughness profile and parameters) was evaluated with a Mitutoyo Surftest SJ-201P portable surface roughness tester. Following DIN EN ISO 4288, a sampling length of 0.8 mm and an evaluation length of 4.0 mm were used for all data acquisition. Three measurements were executed in the stable region for each run, and the mean values of the results were used for representing the average (R_a) and total (R_t) roughness values.

In this work, the influences of the main machining parameters (cutting speed v_c, feed per tooth f_z, and axial depth of cut a_p) were tested in three levels, according to Table 2. The experimental procedure followed the BBD, with 15 runs executed randomly (Table 3). The variance analysis (ANOVA) allowed the evaluation of the main effects and the contributions of each control variable (v_c, f_z, a_p) in the response variables (F_U, dF_U, R_a, R_t) in the end milling of wear-resistant steel Hardox® 450. The BBD describes the optimal levels of these input variables to achieve minimum levels simultaneously for all output variables.

Table 2: Cutting parameters and levels.

Controllable Input Factors	**Levels**		
	Low (-1)	Middle (0)	High (+1)
v_c (m/min)	60	90	120
f_z (mm/tooth)	0.08	0.10	0.12
a_p (mm)	0.2	0.4	0.6

Source: Authors, (2022).

The machined surface and tool wear images were monitored using a Dino-Lite AM 413ZT USB digital microscope with a magnification of 50x.

III. RESULTS AND DISCUSSIONS

Table 3 presents the output factors as a function of the input parameters. The input parameters were only repeated in runs 3, 8, and 14. Since all factors were evaluated at the intermediary level (0), these runs will be considered middle points. The ratio between dF_U and F_U varied between 0.21 and 0.56, indicating that the experiments occurred in a stable regimen. According to Sória [19], milling becomes unstable when $dF_U > F_U$, resulting in vibrations that could affect the quality of the machined surface.

Table 3: Response variables as a function of the controllable factors.

Run Order	Controllable Factors			Response Variables					
	v_c (m/min)	f_z (mm/tooth)	a_p (mm)	F_a (N)	F_p (N)	F_U (N)	dF_U (N)	R_a (µm)	R_t (µm)
1	60	0.10	0.20	47.1	50.5	59.8	34.2	1.73	12.3
2	90	0.12	0.60	143.9	102.3	176.6	70.9	3.40	23.8
3*	90	0.10	0.40	83.9	94.3	126.2	45.2	0.43	2.0
4	60	0.08	0.40	98.7	81.3	127.9	79.9	2.48	17.3
5	120	0.10	0.20	62.6	123.5	138.5	55.1	0.75	4.9
6	60	0.10	0.60	148.1	114.2	187.1	60.6	2.53	14.9
7	120	0.10	0.60	151.4	124.4	196.0	71.7	2.42	13.4
8*	90	0.10	0.40	102.5	125.1	161.7	47.4	0.57	3.1
9	90	0.08	0.20	46.0	78.6	91.0	53.0	0.75	4.1
10	90	0.12	0.20	70.5	118.8	138.1	50.5	0.60	4.5
11	90	0.08	0.60	147.8	158.0	216.4	51.1	1.45	8.9
12	120	0.12	0.40	113.3	160.0	196.1	50.1	0.63	3.6
13	60	0.12	0.40	129.8	118.7	175.9	53.4	1.85	10.1
14*	90	0.10	0.40	129.6	162.1	207.6	54.6	0.62	3.9
15	120	0.08	0.40	121.2	188.7	224.3	64.4	0.52	4.3

*Central level runs defined by BBD from middle points (0).
Source: Authors, (2022)

III.1 RESULTING FORCE

Figure 3 displays the static (F_U) and dynamic (dF_U) force values obtained in the experiments. An increase in F_U was observed in the middle points, probably due to the premature tool wear throughout the experiment. Another phenomenon observed is that starting from run 8, dF_U remains well-nigh constant (53 ± 5 N) until the end of the study, indicating a disturbance during material cutting, possibly related to the tool wear.

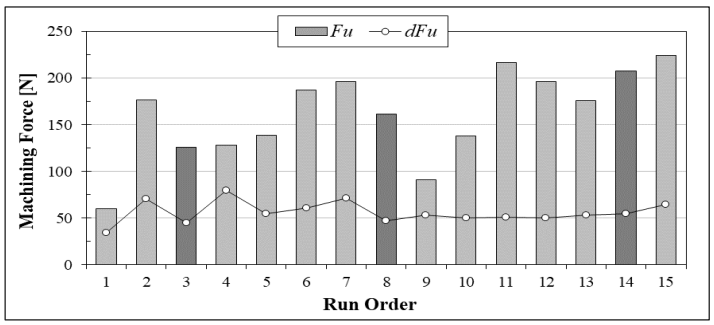

Figure 3: Static (F_U) and dynamic (dF_U) force values measured in each run.
Source: Authors, (2022).

Figure 4 presents the active and passive components of the machining force. The passive force (F_p) presented a tendency to be higher than the active force (F_a). The exceptions were runs 2, 4, 6, and 7. While runs 2, 6, and 7 correspond to cutting conditions with the highest a_p level, a high dF_U was observed in run 4, indicating significant force fluctuation. This oscillation may be associated with the difficulty of chip shearing (due to the low width of cut) and work hardening, and high R_a and R_t values are also expected [20]. Moreover, $F_p \cong 2\,F_a$ in run 5 due to the small a_p/r_ε ratio increases the passive force [19]. This fact is also observed in runs 9 and 10, where $a_p = 0.5\,r_\varepsilon$. This effect was slightly evident in run 1, possibly due to the new cutting edge combined with a low cutting speed (60 m/min).

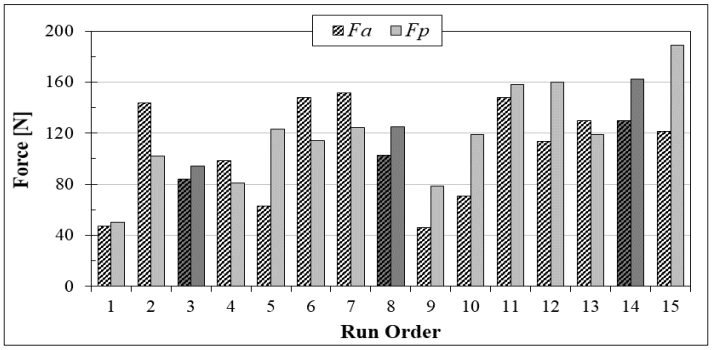

Figure 4: Active (F_a) and passive (F_p) force values measured in each run.
Source: Authors, (2022).

Figure 5 presents images of the cutting edge after runs 6, 12, and 15 to illustrate the progression of the flank wear. Despite being only a qualitative analysis of the tool wear, the increase in the force values between the middle points (runs 3, 8, and 14) and the visual examination of the insert suggests that the machining of Hardox® 450 with PK35 CVD-coated carbide inserts leads to premature tool wear. This phenomenon was unexpected: Majerik and Danisova (2010) evaluated the tool-life of coated carbide tools in rough milling of Hardox® 500 under similar conditions, finding tool lives over 120 min, much higher than the sum of all the 15 runs performed with Hardox® 450. Majerik and Barenyi (2016) estimated a tool life of 78.5 min for the end milling of Hardox® 500 with coated carbide tools with a cutting speed of 135 m/min.

III.2 AVERAGE AND TOTAL ROUGHNESS

Figure 6 presents the average roughness (R_a) and Figure 7 the total roughness (R_t) values by end milling of Hardox® 450. Both roughness parameters presented low values at the middle points and exhibited similar behaviors ($R_t \cong 6\,R_a$). The highest values of R_a and R_t were observed in the sampled machined in Run 2. This

sample also presents the highest dispersion in R_a, which is related to the severe configuration of this run: f_z and a_p at the high levels and v_c at the medium level.

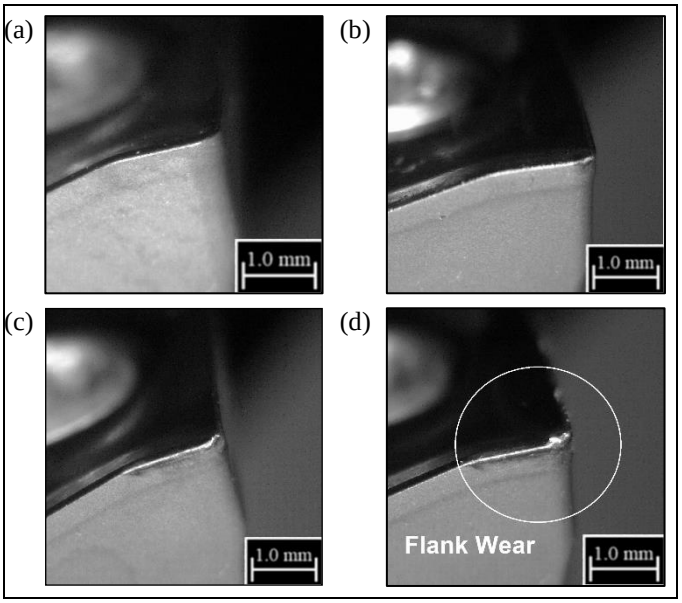

Figure 5: Tool wear monitoring throughout the experiment: (a) new tool; (b) after run 6; (c) after run 12; (d) after run 15.
Source: Authors, (2022).

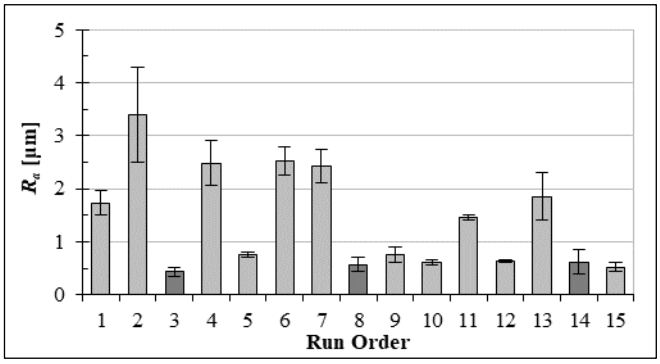

Figure 6: Average roughness R_a values of machined samples
Source: Authors, (2022).

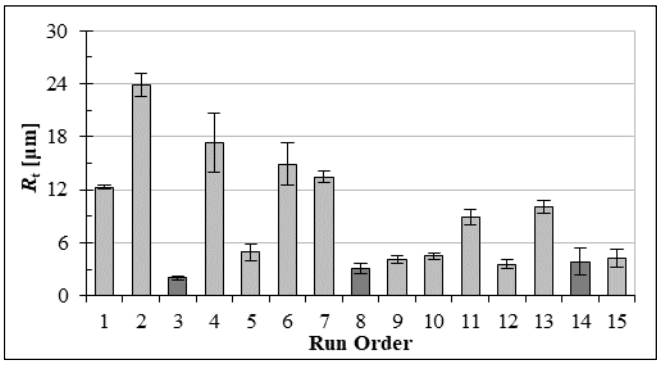

Figure 7: Total roughness R_t values of machined samples.
Source: Authors, (2022).

It is common knowledge that, in machining processes, the surface roughness is mainly affected by feed rate (or feed per tooth, for multiple cutting edges). However, significant differences were observed between runs performed with the same feed per tooth. Figure 8 illustrates the surface profiles and images of the respective surfaces machined with f_z = 0.1 mm/rev. Figure 8a presents the surface profile for run 3 (v_c = 90 m/min, a_p = 0,4 mm): this run presented the lowest roughness values in both parameters considered, and the machined surface exhibits well-defined feed-per-tooth marks produced by the cutting tool (Figure 8c). The roughness profile of sample 6 (Figure 8b) presents much higher with irregular peaks and valleys, with some discernible undulation. The image of the surface machined in this test (Figure 8d) does not present a regular pattern, indicating a possible difficulty for the chip breakage, leading to burr formation and increasing the measured roughness. According to Chinchanikar and Choudhury [22], this difficulty is related to the low v_c, and, under low f_z, lower cutting speeds tend to increase the surface roughness of the machined parts. Another possible explanation is the occurrence of unstable built-up edge (BUE); however, no adherence was identified in the periodic tool evaluations.

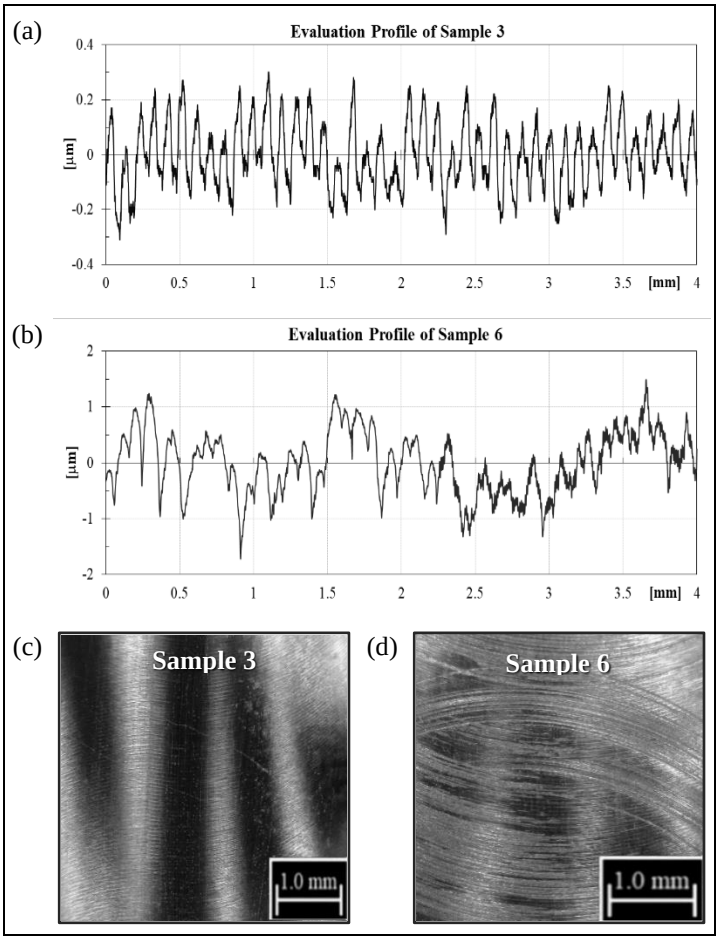

Figure 8: Roughness profiles and images of the machined surface after runs 3 and 6.
Source: Authors, (2022).

III.3 STATISTICAL ANALYSIS

Table 4 presents the reduced ANOVA of the response variables considering a 95% confidence interval. Furthermore, the effect was considered partially significant for a confidence interval between 90 and 95%. According to Montgomery and Hunger [17], one may consider that the statistical model represents well the behavior of the response variable when the coefficient of determination (R^2) is higher than 70%, which was observed for all the cases. The regression models obtained for each parameter are presented in equations 5 to 8.

Table 4: Reduced ANOVA of the main effects.

Factor	F_U [N]		dF_U [N]		R_a [µm]		R_t [µm]	
	p-value	Cont. (%)	p-value	Cont. (%)	p-value	Cont. (%)	p-value	Cont. (%)
v_c	0.016	17.3	-	-	0.034	17.7	0.079	17.5
a_p	0.001	48.1	0.005	38.0	0.010	34.6	0.042	27.0
v_c^2	–	–	0.125	6.50	0.091	7.20	0.208	5.50
a_p^2	0.097	7.0	0.026	19.7	0.040	16.0	0.092	15.7
f_z x a_p	0.100	6.8	0.158	6.76	0.100	8.60	0.173	9.14
R^2	72.4%		70.9%		89.4%		81.9%	

Source: Authors, (2022).

$$F_U = 174.9 + 24.77\ v_c + 41.27\ a_p - 0.1\ v_c^2 - 23.0\ a_p^2 - 21.9\ f_z\ x\ a_p \quad (5)$$

$$dF_U = 45.4 + 2.22\ v_c + 8.27\ a_p + 5.63\ v_c^2 + 8.74\ a_p^2 + 4.94\ f_z\ x\ a_p \quad (6)$$

$$R_a = 0.701 - 0.534\ v_c + 0.746\ a_p + 0.549\ v_c^2 + 0.729\ a_p^2 + 0.525\ f_z\ x\ a_p \quad (7)$$

$$R_t = 4.47 - 3.55\ v_c + 4.40\ a_p + 3.25\ v_c^2 + 4.75\ a_p^2 + 3.63\ f_z\ x\ a_p \quad (8)$$

The linear effect of the axial depth of cut (a_p) presented the most significant influence for all the response variables evaluated. The quadratic effect (a_p^2) was significant for the dynamic force (dF_U) and R_a and partially significant for the static force (F_U). The linear effect of the cutting speed (v_c) also presented a significant contribution to F_U, partially significant for R_t, while v_c^2 had a partially significant influence over dF_U, R_a, and R_t. The only interaction effect that showed some degree of influence (i.e., partially significant) on the response variables was f_z x a_p.

Figure 9 presents contour plots for the static (F_U) and dynamic (dF_U) forces as a function of f_z x v_c for the three tested levels of a_p (most significant parameter). Distinct behaviors were observed for F_U and dF_U with the increase of a_p: for $a_p \leq r_\varepsilon$ (Figures 9a and 9b), F_U increases with v_c and f_z. This behavior is related to the increased cross-section of the cut with higher feed rates that directly affect F_U. However, for $a_p = 1.5\ r_\varepsilon$ (Figure 9c), F_U increases with higher cutting speeds and decreases with higher levels of feed per tooth. In this case, there is a strong influence of f_z on the generated chip: the combination of thin chips with high a_p hampers material shearing, leading the chip to be crushed instead of sheared. As a result of the characteristics of the Hardox® 450, this heightens work hardening, leading to higher machining forces.

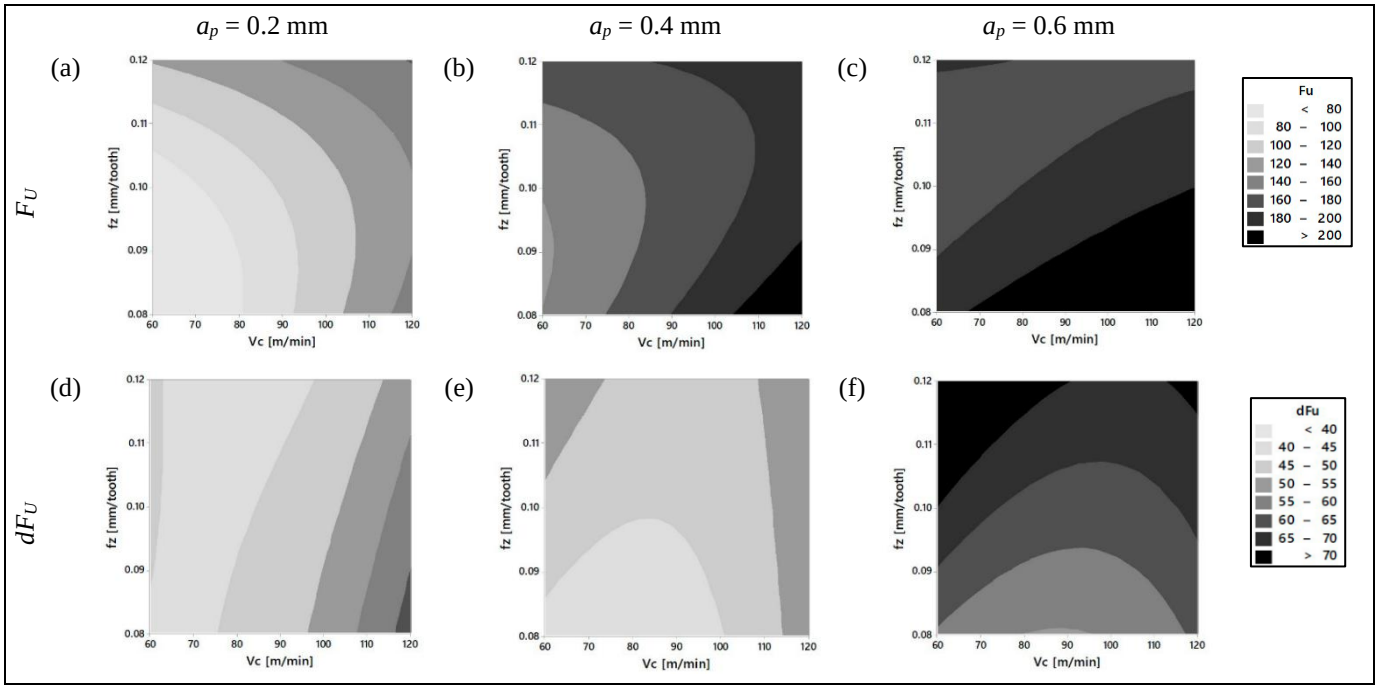

Figure 9: Contour plots of F_U and dF_U for a_p= 0.2 mm; 0.4 mm; 0.6 mm.
Source: Authors, (2022).

Feed per tooth presented a low influence on the dynamic force for a_p = 0.2 mm (Figure 9d). For $a_p \geq r_\varepsilon$ (Figures 9e and 9f), the influence of the quadratic effect of the cutting speed is evident, with the v_c x f_z contour lines following parabolic-like curves. The analysis of the contour plots indicates more severe regions (higher dF_U) as f_z increases and v_c departs from 90 m/min. This effect may reveal possible instability regions at the extremes (60 and 120 m/min) with $a_p \geq 0.4$ mm [19].

According to Table 4, the linear effect of a_p has the most significant influence on R_a and R_t, followed by the linear effect of

v_c. Except for v_c for R_t, the quadratic effects of v_c and a_p and the interaction f_z x a_p showed significant influence on R_a and R_t for a confidence interval of 90% or higher. The contour plots in Figure 10 confirm these results, where the behaviors of R_a and R_t curves are very similar for each level of a_p. The regions with lower roughness values are dislocated for different levels of a_p. For a_p = 0.5 r_ε (Figures 10a and 10d), the combination of low v_c and f_z produces higher R_a and R_t values due to the difficult chip cutting and subsequent burr formation on the machined surface [22]. Consequently, a better surface finish is achieved with higher values of v_c and f_z, with the low roughness region located in the upper limit of the studied domain. For $a_p \geq r_\varepsilon$ (0.4 e 0.6 mm), the plot behaviors are similar and, as expected, the roughness values increase with the growth of f_z and with the decrease of v_c [19]; however, the center of the low roughness region has been dislocated to the lower tested value of the feed per tooth.

The analysis of the surface roughness of the samples machined in the middle points (runs 3, 8, and 14) indicates a slight increase of R_a and R_t mean values throughout the experiment. However, the dispersions of the roughness values increased significantly during the experiment, indicating a stronger influence of the tool wear over these dispersions.

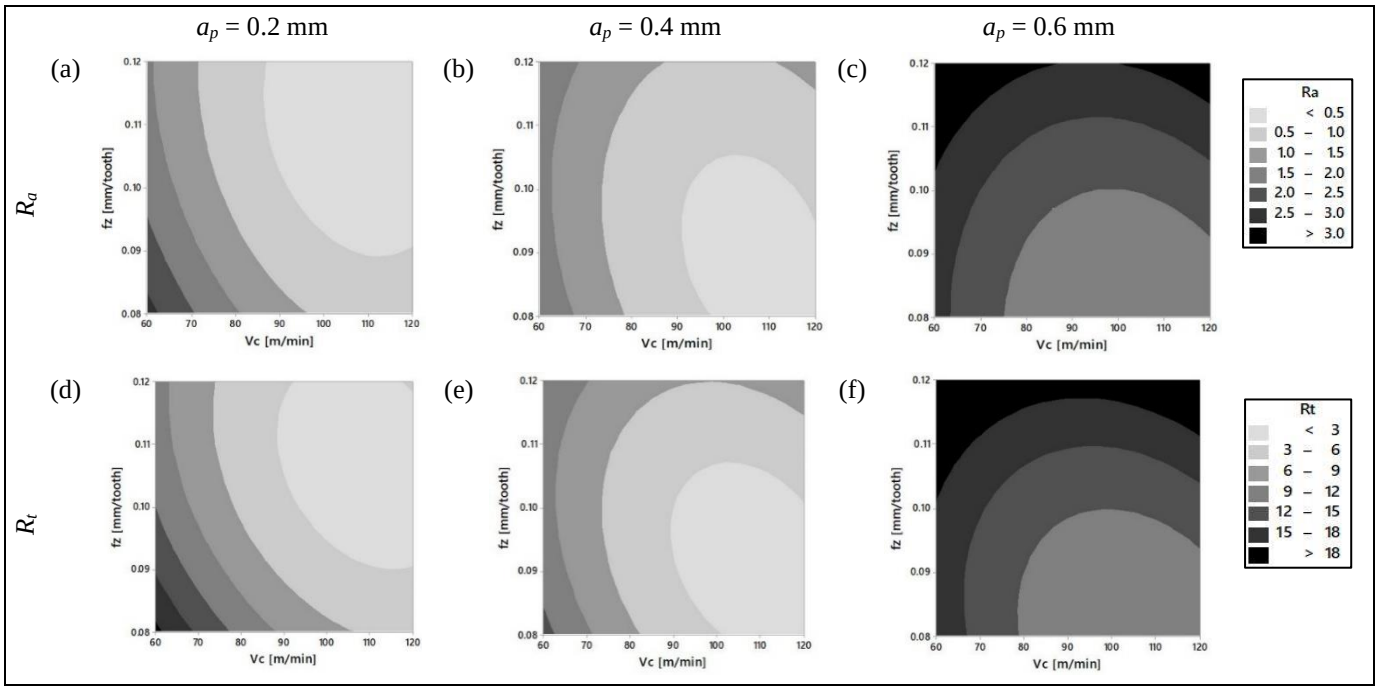

Figure 10: Contour plots of R_a and R_t for a_p= 0.2 mm; 0.4 mm; 0.6 mm.
Source: Authors, (2022).

III.4. MULTIOBJECTIVE OPTIMIZATION OF CUTTING PARAMETERS

Figure 11 illustrates the characteristic curves of each controllable input factor (v_c, f_z, a_p) on the response variables (F_U, dF_U, R_a, R_t). The optimized input variables are indicated through vertical lines, and the predictions of response values are presented utilizing the dashed horizontal line. It is observed that a_p is the only parameter whose value chosen for the optimization is on the vicinities of the lower level (0.212 mm), while the choice of the values of v_c and f_z approached the average tested values (89.1 m/min and 0.103 mm/tooth respectively). The behavior of R_a and R_t was similar for all variables, indicating the same optimization points. The same does not apply in terms of the comparison between F_U and dF_U. The result of "composite desirability" (D) presented a suitable value, considering that it seeks to optimize four simultaneous parameters. In contrast, the "individual desirabilities" (d) of the roughness parameters were close to the ideal (d = 1), and the forces presented acceptable values [15].

The results of the validation test are presented in Table 5. The validation test returned a lower static force and a higher dynamic force when compared to the values predicted by equations 3 and 4. These differences were expected since the models presented determination coefficients in the boundaries of the acceptable ($R^2 \cong 70\%$) due to disturbances that reduced the cutting stability and tool wear, affecting the force values.

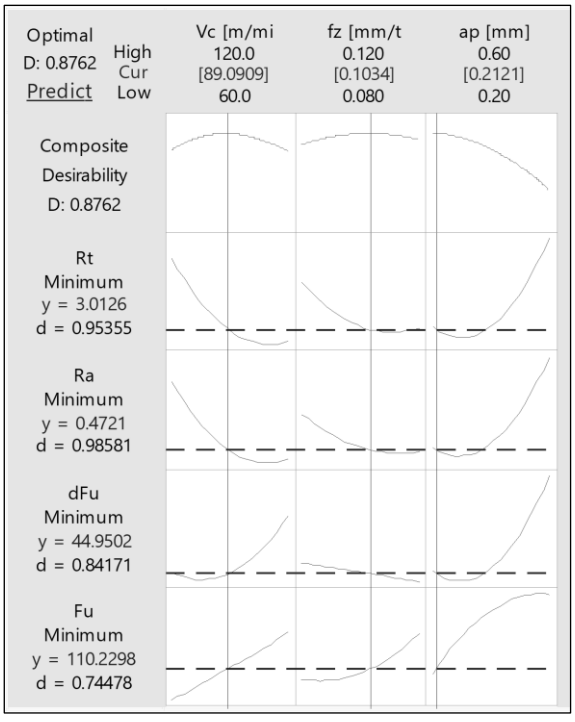

Figure 11: Characteristic curves of controllable factors.
Source: Authors, (2022).

Table 5: Validation of multiobjective optimization.

	F_U [N]	dF_U [N]	R_a [µm]	R_t [µm]
Predicted	110	45	0.47	3.01
Measured	96	65	0.57	4.24

Source: Authors, (2022).

The roughness values predicted by equations 5 and 6 were lower than the validation results. Equation 5 presented a good prediction for R_a, considering diverse factors like vibration and tool wear could affect the measured values [16]. Although the difference between the predicted and measured R_t values is high, this parameter is the most sensitive to texture variations since it comprises the maximum peak-to-valley height in the evaluation length of the roughness profile.

The multiobjective optimization reached output values considerably low relating to those obtained previously. The different behaviors observed can still be considered efficient in the combined minimization of response variables.

IV. CONCLUSIONS

Multiobjective optimization of cutting parameters (cutting speed v_c, axial depth of cut a_p, and feed per tooth f_z) was performed for the end milling of wear-resistant steel Hardox® 450 using CVD-coated carbide tools. Static and dynamic machining forces (F_U and dF_U) and average and total roughness values (R_a and R_t) were analyzed, leading to the following conclusions:

- The lowest F_U value was registered on the first run (new insert) with the lowest v_c and a_p levels and the intermediate f_z level.
- A tendency of increasing F_U values throughout the experiment was observed in the analysis of the middle points (runs 3, 8, and 14). F_U presented steady growth by the replications of this condition due to tool wear. This effect was observed on a smaller scale for dF_U.
- For a 95% confidence interval, the reduced ANOVA indicated a statistically significant influence of the linear effects of v_c and a_p on F_U, while dF_U was only significantly influenced by a_p (linear and quadratic effects).
- The surface roughness parameters R_a and R_t did not seem to have been strongly affected by the tool wear. However, the increasing dispersion of the values measured along the middle-point replications suggests that the tool wear somehow influences the surface finish of the machined parts.
- The reduced ANOVA also showed a significant influence of a_p on R_a and R_t for a 95% confidence interval. Both v_c and the quadratic effect of a_p significantly influenced R_a.
- According to the multiobjective optimization, best results (minimum levels of all response variables) are obtained with a_p close to the lowest tested level (0.212 mm), while v_c and f_z must be kept close to the medium applied levels (89.1 m/min and 0.103 mm/tooth).
- Differences between the predicted and measured values during validation can be attributed to noncontrollable input factors, such as tool wear; however, both forces and roughness values were considerably low throughout the experiment.
- A more in-deep study on the influence of tool wear over the response variables is recommended since it may increase the force components and cause vibrations; detailed investigations regarding chip formation in the end milling of Hardox® 450 are also suggested.

V. AUTHOR'S CONTRIBUTION

Conceptualization: Émerson S. Passari and André J. Souza.
Methodology: Émerson S. Passari and André J. Souza.
Investigation: Émerson S. Passari and André J. Souza.
Discussion of results: Émerson S. Passari, Heraldo J. Amorim and André J. Souza.
Writing – Original Draft: Émerson S. Passari.
Writing – Review and Editing: Heraldo J. Amorim and André J. Souza.
Resources: (not applicable).
Supervision: Heraldo J. Amorim and André J. Souza.
Approval of the final text: Émerson S. Passari, Heraldo J. Amorim and André J. Souza.

VI. ACKNOWLEDGMENTS

The authors thank SSAB/SC Co. for donating the Hardox® 450 steel plate, Walter Tools for coated carbide inserts, Bondmann Chemical Industry for cutting fluid, and Coordenação de Aperfeiçoamento de Pessoal de Nível Superior – Capes (Grant No. 495511/2020-00) for the graduate scholarship.

VII. REFERENCES

[1] SSAB, Hardox® 450 Data Sheet 168uk., 2021. https://www.ssab.com/products/brands/hardox/products/hardox-450. Accessed 16 June 2021.

[2] Gallina, B., Biehl, L. V., Medeiros, J. L. B. et al., "The influence of different heat treatment cycles on the properties of the steels HARDOX® 500 and STRENX® 700." Rev Liberato (Online), vol. 21, no. 35, pp. 67-74, 2020. http://revista.liberato.com.br/index.php/revista/article/view/640.

[3] Duc, T. M., Long, T. T., Thanh, D. V., "Evaluation of minimum quantity lubrication and minimum quantity cooling lubrication performance in hard drilling of Hardox 500 steel using Al_2O_3 nanofluid." Adv Mech Eng, vol. 12, no. 2, pp. 1-12, 2020. https://doi.org/10.1177/1687814019888404.

[4] Klocke, F., Manufacturing Processes 1 – Cutting. Springer-Verlag, Berlin Heidelberg, 2011. https://doi.org/10.1007/978-3-642-11979-8.

[5] SSAB., Cutting of HARDOX wear plate, Hardox® TechSupport #16, 2007. https://www.aemach.com/hardox/hardox_working.htm. Accessed 10 March 2021.

[6] Stonkus, E., "Research of heat affected zone after cutting in Hardox steel." Dissertation, Kaunas University of Technology, Lithuania, 2015. https://epubl.ktu.edu/object/elaba:8666130.

[7] Perec, A., Musial, W., Prazmo, J. et al., "Multi-criteria optimization of the abrasive waterjet cutting process for the high-strength and wear-resistant steel Hardox®500." In: Klichová D et al. (eds) Advances in Water Jetting, Springer, Cham., 2021. https://doi.org/10.1007/978-3-030-53491-2_16.

[8] Kar, B. C., Panda, A., Kumar, R. et al., "Research trends in high-speed milling of metal alloys: A short review." Mater Today: Proc, vol. 26, no. 2, pp. 2657-2662, 2020. https://doi.org/10.1016/j.matpr.2020.02.559.

[9] Krolczyk, G. M., Krolczyk, J. B., Maruda, R. W. et al., "Metrological changes in surface morphology of high-strength steels in manufacturing processes." Meas, vol. 88, pp. 176-185, 2016. https://doi.org/10.1016/j.measurement.2016.03.055.

[10] Daniyan, I. A., Tlhabadira, I., Mpofu, K. et al., "Process design and optimization for the milling operation of aluminum alloy (AA6063 T6)." Mater Today: Proc, vol. 32, no. 2, pp. 536-542, 2021. https://doi.org/10.1016/j.matpr.2020.02.396.

[11] Jayaraman, P., Mahesh Kumar, L., "Multi-response optimization of machining parameters of turning AA6063 T6 aluminium alloy using Grey Relational Analysis in Taguchi Method. Procedia Eng, vol. 97, pp. 197-204, 2014. https://doi.org/10.1016/j.proeng.2014.12.242.

[12] Kara, F., "Optimization of cutting parameters in finishing milling of Hardox 400 steel." IJAEFEA, vol. 5, no. 3, pp. 44-49, 2018. https://doi.org/10.26706/IJAEFEA.3.5.20180901.

[13] Moayyedian, M., Mohajer, A., Kazemian, M. G. et al. "Surface roughness analysis in milling machining using design of experiment." SN Appl Sci, vol. 2, pp. 1698, 2020. https://doi.org/10.1007/s42452-020-03485-5.

[14] Nekere, M. L., Singh, A. P., "Optimization of aluminium blank sand casting process by using Taguchi's robust design method." Int. J. Qual. Res., vol. 6, no. 1, pp. 81-97, 2012. http://www.ijqr.net/journal/v6-n1/10.pdf.

[15] Myers, R. H., Montgomery, D. C., Anderson-Cook, C. M. "Response surface methodology: process and product optimization using designed experiments", 4 ed. Wiley, Hoboken, 2016.

[16] Policena, M. R., Devitte, C., Fronza, G. et al. "Surface roughness analysis in finishing end-milling of duplex stainless steel UNS S32205." Int J Adv Manuf Syst, vol. 98, pp. 1617-1625, 2018. https://doi.org/10.1007/s00170-018-2356-4.

[17] Montgomery, D. C., Hunger, G. C., "Applied statistics and probability for engineers", 7 ed. Wiley, Hoboken, 2018.

[18] Hübner, H. B., Souza, A. J. "Evaluation of machining forces in asymmetrical face milling of cast iron DIN GGG50." Key Eng Mater, vol. 656-657, pp. 271-276, 2015. https://doi.org/10.4028/www.scientific.net/KEM.656-657.271.

[19] Sória, B. S., "Study of vibration behavior in end milling of AISI 316 stainless steel using Wavelet transform." Dissertation, Federal University of Rio Grande do Sul, Brazil (in Portuguese), 2016. https://www.lume.ufrgs.br/handle/10183/152768.

[20] Majerik, J., Barenyi, I., "Experimental investigation of tool wear cemented carbide cutting inserts when machining wear-resistant steel Hardox 500." Eng Rev vol. 36, no. 2, pp. 167-174, 2016. https://hrcak.srce.hr/155321.

[21] Majerik, J., Danisova, N., "Experimental testing methods of Hardox 500 face milling by Pramet 8230 carbide inserts." Ann Fac Eng Hunedoara (Online) vol. 8, no. 3, pp. 263-266, 2010. http://annals.fih.upt.ro/pdf-full/2010/ANNALS-2010-3-53.pdf

[22] Chinchanikar, S., Choudhury, S. K., "Effect of work material hardness and cutting parameters on performance of coated carbide tool when turning hardened steel: An optimization approach." Meas, vol. 46, no. 4, pp. 1572-1584, 2013. https://doi.org/10.1016/j.measurement.2012.11.032.